Open Archive Toulouse Archive Ouverte (OATAO)

OATAO is an open access repository that collects the work of Toulouse researchers and makes it freely available over the web where possible

This is an author's version published in: **http://oatao.univ-toulouse.fr/20492**

Halotolerant bioanodes: The applied potential modulates the electrochemical characteristics, the biofilm structure and the ratio of the two dominant genera

Raphaël Rousseau [a], Catherine Santaella [b], Anaïs Bonnafous [c], Wafa Achouak [b], Jean-Jacques Godon [c], Marie-Line Delia [a], Alain Bergel [a,*]

[a] Laboratoire de Génie Chimique, CNRS-Université de Toulouse (INPT), 4 allée Emile Monso, BP 84234, 31432 Toulouse, France
[b] Laboratoire d'Ecologie Microbienne de la Rhizosphère & Environnement Extrêmes (LEMiRE), UMR 7265, CNRS-CEA-Aix-Marseille, Université, CEA Cadarache DSV/IBEB/SBVME, 13108 Saint Paul lez Durance, France
[c] INRA UR 0050, Laboratoire de Biotechnologie de l'Environnement, Avenue des Etangs, F-11100 Narbonne, France

ARTICLE INFO

ABSTRACT

The development of economically-efficient microbial electrochemical technologies remains hindered by the low ionic conductivity of the culture media used as the electrolyte. To overcome this drawback, halotolerant bioanodes were designed with salt marsh sediment used as the inoculum in electrolytes containing NaCl at 30 or 45 g/L (ionic conductivity 7.0 or 10.4 $S \cdot m^{-1}$). The bioanodes were formed at four different potentials -0.4, -0.2, 0.0 and 0.2 V/SCE to identify the effect on the electrochemical kinetic parameters, the biofilm structures and the composition of the microbial communities. The bioanodes formed at -0.4 V/SCE were largely dominated by *Marinobacter* spp. Voltammetry showed that they provided higher currents than the other bioanodes in the range of low potentials, but the maximum currents were limited by the poor surface colonization. The bioanodes formed at -0.2, 0.0 and 0.2 V/SCE showed similar ratios of *Marinobacter* and *Desulfuromonas* spp. and higher values of the maximum current density. The combined analysis of kinetic parameters, biofilm structure and biofilm composition showed that *Marinobacter* spp., which ensured a higher electron transfer rate, were promising species for the design of halotolerant bioanodes. The challenge is now to overcome its limited surface colonization in the absence of *Desulfuromonas* spp.

1. Introduction

In the past decade, the association of microbial catalysis with electrochemistry has given rise to a huge number of innovative processes, which may impact a large variety of application domains such as energy production, wastewater treatment, synthesis of biocommodities, biosensing, metal recovery, etc. [1,2]. Microbial anodes are at the core of most of these microbial electrochemical technologies (METs) and very many studies have been dedicated to their design [3]. It is now possible to obtain efficient microbial anodes on carbon [4,5], which reach the current limiting plateau at potential so low as 0.0 V/SHE, and on stainless steel electrodes [6,7] and other metallic materials [8]. Multilayer structures have been shown to produce up to 390 A/m² at 0.39 V/SHE [9] for the oxidation of acetate.

Unfortunately, nothing is perfect. The microbial anodes that have produced the highest currents so far do not tolerate high salinities and operate only in solutions of low ionic conductivity, generally <2 $S \cdot m^{-1}$. For comparison, conventional, abiotic, commercial processes, e.g. hydrogen production by water electrolysis, commonly implement electrolytes of conductivity around 20 $S \cdot m^{-1}$ and up to 60 $S \cdot m^{-1}$ (KOH 33% by mass). A reactor with an inter-electrode distance of 2 cm working with a current density of 200 $A \cdot m^{-2}$ must overcome an ohmic drop of only 67 mV when operating with an electrolyte of 60 $S \cdot m^{-1}$ conductivity, while the ohmic drop would reach the considerable value of 2000 mV with an electrolyte of 2 $S \cdot m^{-1}$ as required to implement microbial anodes. The energy loss due to ohmic drop through the electrolyte can be multiplied by a factor of 30 when a microbial anode is substituted for a conventional abiotic anode. It should be mentioned that this numerical illustration is realistic with regard to the state of the art: a current density of 200 A/m² has been reached recently by the most efficient microbial anodes [9], and the commercial, abiotic water electrolysis units easily ensure higher values.

In summary, microbial anodes are starting to become efficient for the oxidation of low-cost organic substrate but they require electrolytes of low ionic conductivity, which precludes operation at high current density. The implementation of microbial anodes in economically efficient industrial reactors is still hindered by the high ohmic drop through the electrolyte. An essential prerequisite for the large-scale

* Corresponding author.
E-mail address: alain.bergel@ensiacet.fr (A. Bergel).

development of METs is consequently to decrease the energy loss due to ohmic drop by designing microbial anodes able to operate in high-salinity electrolytes.

Our previous work has presented the design of efficient microbial anodes that operate in highly saline electrolytes, using salt marsh sediment as the inoculum. Up to 85 A·m^{-2} have thus been produced at 0.1 V/SCE applied potential, in solutions containing 45 g·L^{-1} NaCl (1.5 times seawater salinity), resulting in an ionic conductivity of 10.4 S·m^{-1} [10]. Surprisingly, all these bioanodes have always revealed the large dominance of only *Marinobacter* and *Desulforomonas* spp.

All the experiments previously reported on these halotolerant microbial anodes were performed with a polarization potential of 0.1 V/SCE [11]. The purpose of the present work was to determine the impact of the polarization potential on the performance and the structure of bioanodes. Bioanodes were formed under well-controlled electrochemical conditions at four different applied potentials ranging from −0.4 to 0.2 V/SCE.

The bioanode kinetics were determined by numerical analysis of the voltammetric records. The architecture of the biofilms was imaged by confocal laser scanning microscopy and the composition of the microbial communities was compared by CE-SSCP fingerprinting and determined by 16S rRNA gene pyrosequencing. It was thus possible to investigate the impact of the applied potential on the electrochemical characteristics of the bioanodes and to link it with the structure of the biofilm and with the ratio of the two dominant microbial genera *Marinobacter* and *Desulfuromonas*. The study illustrates the suitability to combine together these three different investigation paths (electrochemistry, biofilm structure and microbial composition) to progress in understanding microbial bioanode mechanisms.

The study may also open up a new research path in the field of microbial corrosion by adding *Marinobacter* spp. to the possible microbial genera involved in biocorrosion mechanisms, as was recently the case for *Geobacter* [12]. Recently, both *Marinobacter* and *Desulfuromonas* spp. have been identified in marine biofilms that induced corrosion of copper alloys [13].

2. Material and methods

2.1. Inoculum and growth medium

Sediments collected from a salt marsh (Mediterranean Sea, Gruissan, France) were used as inoculum. Conductivity from 7.6 to 12.3 S·m^{-1} and pH from 6.5 to 7.4 were measured in situ. A volume of 200 mL of sediments was mixed with 1800 mL of a culture medium based on the Starkey medium (NH$_4$Cl 2 g·L^{-1}, K$_2$HPO$_4$ 0.5 g·L^{-1}, NaCH$_3$COO 40 mM, HCl 37% 46 mL, MgCl$_2$·6H$_2$O 55 mg·L^{-1}, FeSO$_4$(NH4)$_2$SO$_4$·6-H$_2$O 7 mg·L^{-1}, ZnCl$_2$·2H$_2$O 1 mg·L^{-1}, MnCl$_2$·4H$_2$O 1.2 mg·L^{-1}, CuSO$_4$·5H$_2$O 0.4 mg·L^{-1}, CoSO$_4$·7H$_2$O 1.3 mg·L^{-1}, BO$_3$H$_3$ 0.1 mg·L^{-1}, Mo$_7$O$_2$(NH4)$_6$·4H$_2$O 1 mg·L^{-1}, NiCl$_2$·6H$_2$O 0.05 mg·L^{-1}, Na$_2$SeO$_3$·5H$_2$O 0.01 mg·L^{-1}, CaCl$_2$.2H$_2$O 60 mg·L^{-1}) with addition of NaCl 30 or 45 g·L^{-1}. The conductivity of the final solution was 7.0 and 10.4 S·m^{-1} with NaCl 30 and 45 g/L, respectively, and its pH was 7.5.

2.2. Electrode and electrochemical procedure

In each experiment, four working electrodes made of 2 cm × 1 cm graphite felt (Mersen, France) were disposed in a circle around a single counter-electrode, which was a 10 cm ∗ 5 cm plate of stainless steel 254 SMO (Outokumpu, Sweden). The working electrodes and counter electrode were electrically connected with a screwed titanium wire (1 mm diameter, Alfa Aesar). A saturated calomel reference electrode (+0.24 V/SHE, Radiometer) was set between the counter and working electrodes. The solution was initially flushed with nitrogen for 20 min. The reactors were in a thermostatic bath maintained at 30 °C. A multichannel potentiostat (Biologic) equipped with an Nstat device allowed each working electrode to be addressed individually. Each electrode was thus polarized at a different potential: - 0.4, −0.2, 0 and 0.2 V/SCE, while being in

the same reactor. The acetate concentration was regularly measured with an enzymatic kit (K-ACETAK, Megazyme). When the concentration fell below 5 to 10 mM, concentrated sodium acetate (4 M) was added to recover the initial 40 mM concentration. After several days of polarization, the potential was relaxed and the microbial anode was left at open circuit until it reached a stable potential. Cyclic voltammetry (1 mV·s^{-1}) was then performed on each anode in the range −0.6 to 0.5 V/SCE. Three successive cycles were performed to check reproducibility. Only the forward scans of the second cycles are presented here.

2.3. Microscopy

A section (0.5 × 0.5 cm^2 about 1 mm thick) was sliced from the surface of the electrodes. The samples were labelled with SYTO® 9 Green Fluorescent Nucleic Acid Stain (Invitrogen), rinsed with sterile water to remove planktonic cells and were mounted between a slide and a CoverWell incubation chamber™ (Invitrogen, 1 or 2 mm thickness).

A FluoView Olympus CLSM microscope equipped with krypton-argon laser (488 nm, 568 nm and 647 nm lines) and objectives LCPPlan 10/XX and LCPlanFL 40/0.60 (working distance 2.3 mm) was used for microscopic observations. Emissions were observed with a 510–560 nm filter on the green channel and 585–640 nm on the red channel. Image stacks were collected every 1 μm. Z-stacks (projection of these images on a plane) were generated using the FluoView software. Three to five random fields were examined using both ×10 and ×40 objectives. Epifluorescence was recorded on an Olympus BX41 equipped with a CytoViVa Dual mode epifluorescence module, with a 150 W halogen light source, and a D350/50× Single Band DAPI Exciter - 25 mm and a S492/18× Single Band FITC Exciter - 25 mm for fluorescence, together with a pre-aligned Koehler illumination device and a visible near infra-red spectrophotometer for diffusion light mode. GraphicConverter X and BioImageL [14] were used for image processing.

2.4. DNA extraction, single strand conformation polymorphism (SSCP) fingerprinting and DNA pyrosequencing

A piece of each electrode (around half of the surface area) was stored at −80 °C in a 2 mL tube (Eppendorf). Genomic DNA was extracted and purified using the protocol described previously [15]. The total DNA extracted was purified using a QiAmp DNA microkit (Qiagen, Hilden, Germany). DNA amount and purity of extracts were confirmed by spectrophotometry (Infinite NanoQuant M200, Tecan, Austria). The bacterial communities were analysed by the PCR–single strand conformation polymorphism (SSCP) fingerprint technique. For SSCP, the highly variable V3 regions of 16S rRNA gene were amplified by PCR from each bioanode DNA sample.

1 μL of genomic DNA sample was amplified by using the primers w49 (5′-ACGGTCCAGACTCCTACGGG-3′, *Escherichia coli* position F330) and 5′-6FAM labelled w104 (5′-TTACCGCGGCTGCTGCTGGCAC-3′, *E. coli* position R533) [16] in accordance with previously described CE-SSCP amplification methods [17]. CE-SSCP electrophoresis was performed with ABI310 (Applied Biosystems) [17]. CE-SSCP profiles were analysed using GeneScan software (Applied Biosystems) and the 'StatFingerprints' package [18]. Pyrosequencing of the DNA samples using a 454 protocol was performed by the Research and Testing Laboratory (Lubbock, USA).

3. Results and discussion

3.1. Electrochemical analysis

3.1.1. Microbial anode formation under constant potential chronoamperometry (CA)

Each electrochemical reactor was equipped with four individually addressed working electrodes, each polarized at a different potential:

−0.40, −0.20, 0.00 and 0.20 V/SCE. These potential values were higher than that of acetate oxidation and low enough to avoid any water oxidation. In the absence of inoculum, none of these potentials resulted in current production. The experiment was reproduced five times in the same conditions. The five experimental runs showed similar current-time evolution to that plotted in Fig. 1A. The initial lag period varied rather largely, from 1 to 4 days, from one experimental run to another. In order to diminish the impact of this experimental deviation, the current densities were measured on each curve 6 days after the current onset. The current densities reported in Fig. 1B at the potentials of −0.4, −0.2, 0.0 and 0.2 V/SCE are the averages of the 5 experimental runs described in the present study. The value for the potential of 0.1 V/SCE was extracted from previously reported experiments, performed with 9 reactors run in identical conditions [11].

Among the 20 bioanodes achieved in the present study and the 9 previous measurements, 19 were formed in electrolytes containing 30 g/L NaCl and 10 with 45 g/L NaCl, without any difference due to salinity. The previous study [11] showed that NaCl concentrations ranging from 30 to 45 g/L led to the formation of similar bioanodes in terms of electrochemical kinetics, biofilm structure and biofilm microbial composition. It was confirmed here that variation of NaCl concentration in the range 30 to 45 g/L did not affect the bioanode behaviour.

Standard deviations on current densities were significant (Fig. 1B). Actually, from one experimental run to another, the current-time curves exhibited the same general trend but the absolute current values were not well reproducible. A similar lack of accurate reproducibility has already been observed when inocula coming from natural environments are used at high inoculation ratio [10,19]. In particular, the large set of experiments used different inoculum samples extracted at different times of the year and an unusual procedure was employed here, which consisted of avoiding substrate depletion. Acetate was added to return to the initial concentration of 40 mM when its concentration decreased to around 5 mM. This procedure succeeded in producing high currents but it introduced some operating differences from one experimental run to another. The current evolutions obtained were consequently less reproducible than the current peaks commonly reported in the literature with successive batches of fresh solution.

Despite the experimental deviation, Fig. 1B shows a clear dependence of the current density on the polarization potential. An exponential variation of the current density with the potential might be expected, according to the Tafel law. Nevertheless, fitting the experimental data by a Tafel law led to parameter values that did not make sense physically (Supplementary data). It can be concluded that the current density provided by the microbial anodes depended on the polarization potential in a complex way that was not straightforwardly controlled by elementary electrochemical kinetics.

3.1.2. Voltammetry

At the end of the chronoamperometry, the anode potential was relaxed. It took about 10 min for the anodes reach a stable open circuit potential (OCP) of −0.50 ± 0.01 V/SCE for all anodes whatever the experimental run. This OCP value was close to the formal potential of the HCO_3^-/CH_3COO^- of −0.56 V/SCE at pH 7.5 (see Supplementary data). The fact that OCP always came back to the same value suggested that identical redox components were present at the electrode/biofilm interface whatever the applied potential used to form the bioanodes.

When OCP was stable, voltammetries were recorded at 1 mV·s^{-1} (Fig. 2). In the zone of low potential of the voltammetry curves, i.e. at potential values below 0.0 V/SCE, the current supplied by the bioanodes formed at −0.4 V/SCE was slightly or significantly higher than the current produced by the bioanodes of the same run formed at 0.0 or 0.2 V/SCE. Over the five experimental runs carried out in this work, this conclusion was verified 4 times (see Table 1 in Supplementary data). A similar observation has already been reported in the literature, leading to the conclusion that a low potential applied during the bioanode formation selects the most efficient electroactive bacteria [20].

In contrast, the high range of potentials showed various situations. The bioanodes formed at −0.4 V/SCE could keep their supremacy or could be surpassed by the bioanodes formed under high potential. This latter case has also already been reported in the literature for microbial anodes formed from pure culture [21] or environmental inoculum [22]. Actually, the pretty complex situation observed here is an illustration of the various observations reported in the literature (see [4] for a review) claiming that the performance of bioanodes can be affected [20,23] or unaffected [24,25] by the potential used to form them.

The voltammetry curves were fitted with the Butler-Volmer-Monod equation, which expresses the current density j as a function of the overpotential η [26]:

$$j = j_{Max} \frac{1 - \exp\left(\frac{-n.F}{R.T}\eta\right)}{K_1 \exp\left(-\frac{(1-\alpha).n.F}{R.T}\eta\right) + K_2 \exp\left(\frac{-n.F}{R.T}\eta\right) + \left(\frac{K_M}{S}+1\right)} \quad (1)$$

where j_{Max} (A·m^{-2}) is the maximum current density, $n = 8$ is the number of electrons produced per mole of acetate, α is the charge transfer coefficient, $F = 96,485$ C·mol^{-1} is the Faraday constant, $R = 8.314$ J mol^{-1} K^{-1} is the universal gas constant, $T = 303$ K is the temperature, K_M (mol·L^{-1}) is the substrate affinity constant, $S = 0.04$ mol·L^{-1} is the substrate concentration, α is the charge transfer coefficient, and K_1 and K_2 are dimensionless parameters.

Five parameters must be numerically adjusted: j_{Max}, K_M, α, K_1 and K_2. Preliminary numerical tests showed that the K_M value did not have
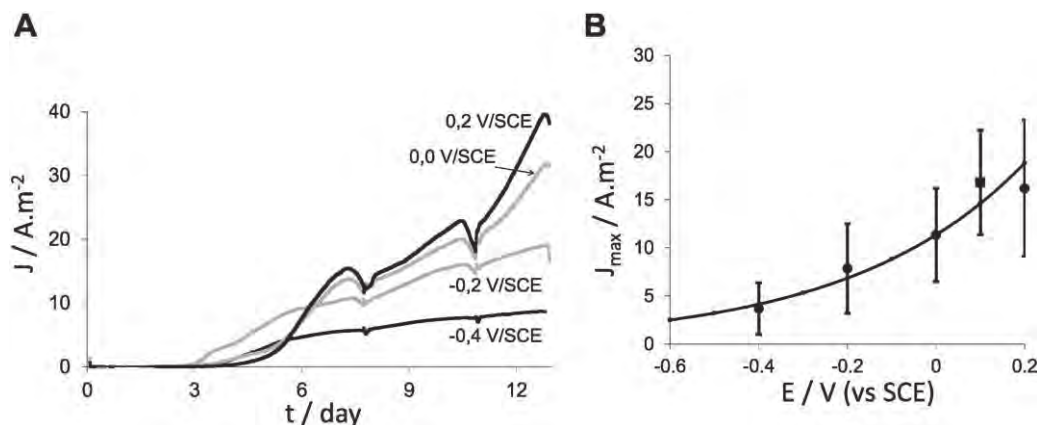
Fig. 1. Chronoamperometries at different polarization potentials. A) Evolution of the current density with time (experimental run #5, performed with 45 g/L NaCl). B) Current densities (J_{max}) recorded 6 days after current onset as a function of the polarization potential (E). Values at −0.4, −0.2, 0.0, and 0.2 V/SCE (circles) were averaged from the 5 experimental runs described here. The average value at 0.1 V/SCE (square) was extracted from 9 previously reported experiments [11].

Fig. 2. Representative set of voltammetric curves recorded with the bioanodes formed at (A) −0.4 V, (B) −0.2 V, (C) 0.0 V and (D) 0.2 V/SCE over 20 days (run #2). The X-axis was plotted in terms of overpotential (η) calculated as the potential E minus open circuit potential. Black lines: experimental, grey lines: Butler-Volmer-Monod model.
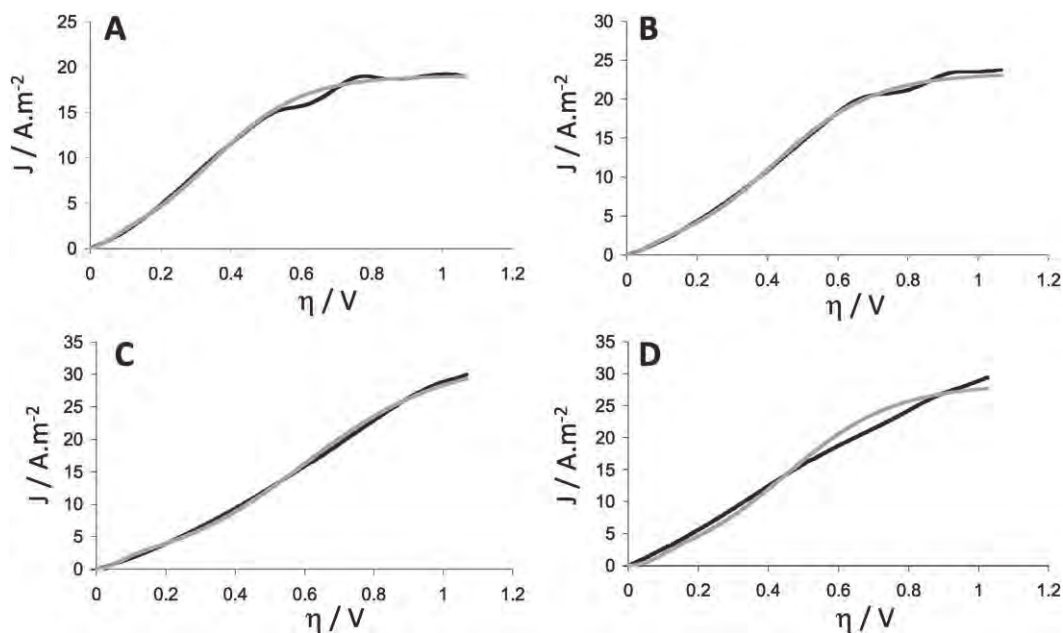
a significant impact in the range from 5 to 8 mM. Experimentally, a fall in current was observed when acetate concentration was less than approximately 10 mM. K_M values of 2.2 mM related to acetate have been reported in the literature [26]. In order to decrease the number of parameters to be adjusted numerically and considering the low impact of K_M, its value was fixed at 5 mM in the further calculations. All the voltammetry curves were thus fitted by adjusting four parameters through least squares regression. The average values obtained on the five experimental runs reported here are gathered together in Table 1.

As observed and commented above for the current densities, standard deviations were also quite high on the adjusted parameters. This is the price to be paid for working with several experimental runs performed at different times and using high ratios of an environmental inoculum. Here, parameter adjustment was based on 20 different curves obtained in 5 independent experimental runs using different samples of the inoculum. In spite of the experimental deviation some clear trends can be extracted.

Firstly, the j_{Max} parameter was significantly lower for the bioanodes formed at −0.4 V/SCE, while it was almost identical for all the others.

The charge transfer coefficient, α, was between 0.8 and 0.9, without any effect of the polarization potential. The same value was found in the previous study carried out at the constant potential of + 0.1 V/SCE [11]. So high α values are unusual for conventional electrochemical reactions, but have already been reported in protein electrochemistry [27]. They pointed out a detrimental dissymmetric energy barrier, which has to

be overcome to transfer the electrons to the electrode. Varying the applied potential did not mitigate this disadvantage.

The K_1 parameter describes how fast the biochemical reactions run relative to the electrochemical reaction [26]. If the electrochemical reaction is extremely fast compared to the biochemical one, K_1 tends to zero and the Butler-Volmer-Monod equation approaches the Nernst-Monod equation. K_1 was considerably lower for −0.4 V/SCE ($K_1 = 12.4$), while it had comparable values at the other potentials, ranging from 20.9 to 27.2. In all the cases, the high values of K_1 indicated that the electron transfer was far from being reversible (Nernstian). Electron transfer to the anode material, rather than the metabolic reactions, was rate-limiting. This trend was enhanced for potential values higher than −0.4 V/SCE, this means that the potential values higher than −0.4 V/SCE either led to less efficient electron transfer or improved the metabolic processes.

The K_2 is expected to be > 1 [26]. This condition was largely validated here. The large variation of K_2 with the applied potential, particularly from −0.4 to 0.0 V/SCE, suggested that the potential used to form the bioanodes impacted the metabolic process. The considerable experimental variation on this parameter should indicate that the metabolic processes were poorly controlled from one reactor to another.

3.2. Architecture of biofilms

Under confocal laser scanning microscopy (CLSM) excitation at 645 nm and photon recovery between 585 and 640 nm yielded visible photoluminescence from the fibres (Fig. 3a). To validate the images obtained in this manner, thin electrode samples were cut that allowed light to pass through. These thin slides imaged in transmission mode (Fig. 3b) confirmed the outlines and shape of the fibre obtained in photoluminescence. The dual mode fluorescence was used, which allows fluorescence and light diffraction to be superimposed. Fig. 3c shows images of graphite felt in dual mode under ultraviolet-blue/green excitation and white light. Graphite felt fibres showed facets resembling those observed in Fig. 3a. Used alone, reflected light microscopy allowed graphite felt to be imaged by hyperspectral microscopy with details of the facets on the fibres (Fig. 3d). Therefore, diffused light accounted for the signal obtained in CLSM. To our knowledge, this is

Table 1
Butler-Volmer-Monod parameters as a function of the polarization potential. Voltammetry curves were recorded at the end of the polarization time and values were averaged from the 5 experimental runs described here. K_M was fixed at 5 mM.

Applied potential during CA (V/SCE)	−0.4	−0.2	0	0.2
j_{Max}	17.5 ± 9.4	37.6 ± 21.1	35.4 ± 16.7	33.8 ± 17.3
α	0.8 ± 0.10	0.8 ± 0.05	0.9 ± 0.05	0.8 ± 0.05
K_1	12.4 ± 3.0	20.9 ± 3.8	27.2 ± 20.5	25.4 ± 17.0
K_2	41.0 ± 18.5	104.2 ± 77.4	196.0 ± 199.2	225.4 ± 222.2

j_{Max} (A.m^{-2}) is the maximum current density, α is the charge transfer coefficient, K_1 and K_2 are dimensionless parameters used in Eq. (1).
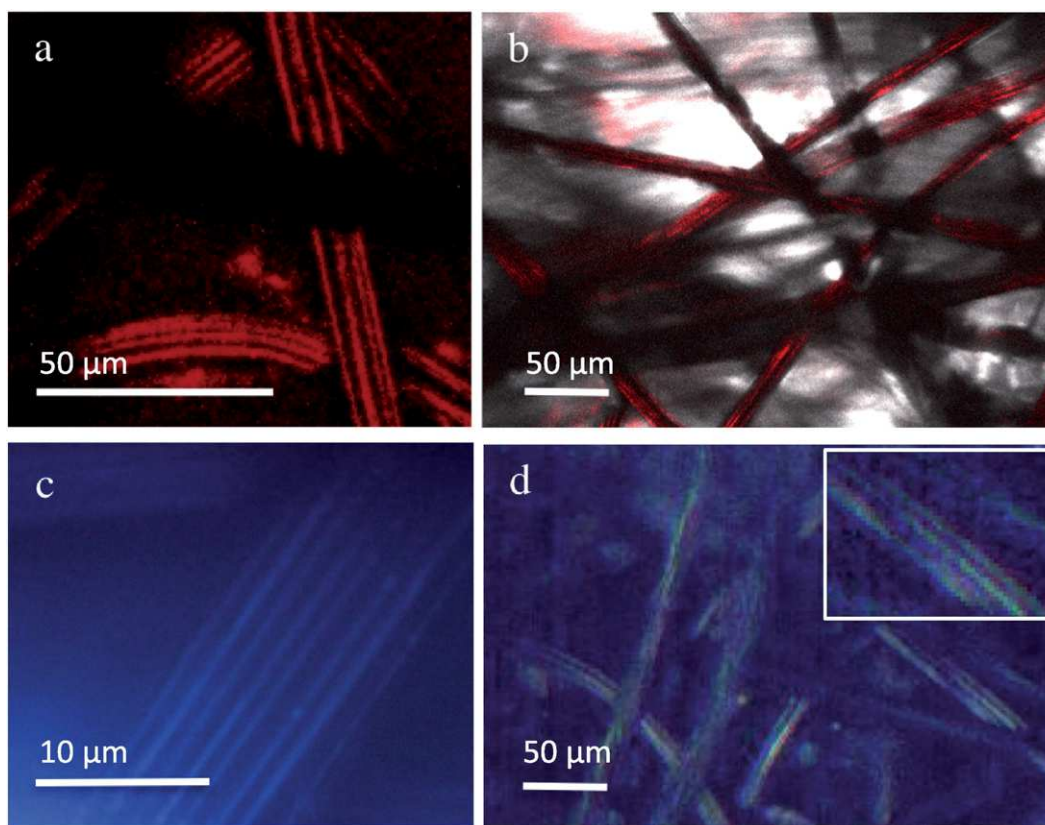
Fig. 3. Imaging of clean graphite felt. a) Excitation 647 nm, emission 585–640 nm, projection of Z-sections through 31 μm. The fibres show straight lines featuring facets; b) Excitation 488 and 647 nm, transmission and emission 585–640 nm on the red channel, projection of Z-sections through 30 μm. The red signal superimposed with graphite felt fibres, as seen in transmission; c) Dual mode epifluorescence, excitation 350 ± 50 nm and white light, graphite felt fibres show facets as in 3a; 3d) Hyperspectral CytoViva® microscopy. The insert top right shows a zoom on a fibre. Graphite felt fibres look similar to those in image a.

the first report of graphite felt imaging in optical microscopy, regardless of transmission or lack of signal in fluorescence.

Fig. 4 gives representative images of the bioanodes developed at −0.4, −0.2, 0.0 and 0.2 V/SCE, which provided current densities of 8, 18, 31, and 39 A/m^2, respectively. The procedure developed here gave the opportunity to image the graphite felt fibres and the biofilm matrix at the same time, which led to unequivocal interpretation of the biofilm structure and development. At the lowest potential (−0.4 V/SCE), the biofilm showed rare, discontinuous, patchy structures near the surface of the fibres (Fig. 4a). The potential of −0.2 V/ECS yielded continuous, thin, dense biofilm layers on the fibres, with thickness near 10 μm (Fig. 4b). Biofilms formed at 0.0 V/SCE showed a diffuse, thick matrix, near 20 μm in thickness, that sheathed the fibres (Fig. 4c). At 0.2 V/SCE, the biofilm displayed a diffuse, fluffy matrix of 30–35 μm thickness that was non-continuous around the fibres and also developed in the spaces between them (Fig. 4d).

In summary, the biofilm architecture was clearly different for the bioanodes formed at −0.4 V/SCE and then it varied according to the applied potential, with a denser volume at higher potentials.

3.3. Microbial populations

CE-SSCP profiles of the electrode samples were recorded for each four bioanodes in the five experimental runs. Representative CE-SSCP profiles are shown in Fig. 5A. Only two main groups of peaks were present on all profiles, indicating that the microbial community of all bioanodes was dominated by the same two major phylotypes.

16S-rRNA gene pyrosequencing of the four bioanodes of an experimental run confirmed the low diversity and indicated that the two peaks detected in CE-SSCP belonged to *Desulfuromonas* and

Marinobacter phylotypes, which represented at least 94% of the biofilm communities for the four bioanodes (Fig. 5B). The other part of the community was made up of various phylotypes, the percentage of each being always <1%. Pyrosequencing replicated for the four bioanodes of another experimental run confirmed these results (Fig. 2 in Supplementary data). The previous work, which was carried out with the single applied potential of 0.1 V/SCE, has also demonstrated the same strong and reproducible selection of these two phylotypes from the extremely large microbial diversity contained in the salt marsh inoculum [11].

For the lowest potential (−0.4 V/SCE) a very low proportion of *Desulfuromonas* was detected, only 5%, while the *Marinobacter* spp. represented 87% of the population (the percentages were 0.3 and 93.5%, respectively for the duplicate in Supplementary data). At the highest potentials, the proportion of *Desulfuromonas* spp. ranged from 39 to 45%. For the highest anode potential (0.2 V/SCE), the *Marinobacter* spp. was dominant, as already observed for bioanodes formed at 0.1 V/SCE [11].

The low abundance of *Desulfuromonas* spp. at the lowest polarization potential indicated that these species had some difficulty in growing when only a limited potential gradient was available between the anode potential and the redox potential of the substrate used as the electron donor. At the other polarization potentials, *Desulfuromonas* spp. competed in a more balanced way against *Marinobacter* spp., even though the *Marinobacter* spp. was generally slightly dominant (5 bioanodes out of 6).

Desulfuromonas species have already been identified as electroactive species, since the pioneering studies [28] and in bioanodes formed from various types of environmental inoculum such as marine sediments [29] or paper mill effluents [30].

Plotting the j$_{Max}$ values, extracted from Butler-Volmer-Monod modelling, against the percentage of *Desulfuromonas* spp. evidenced a
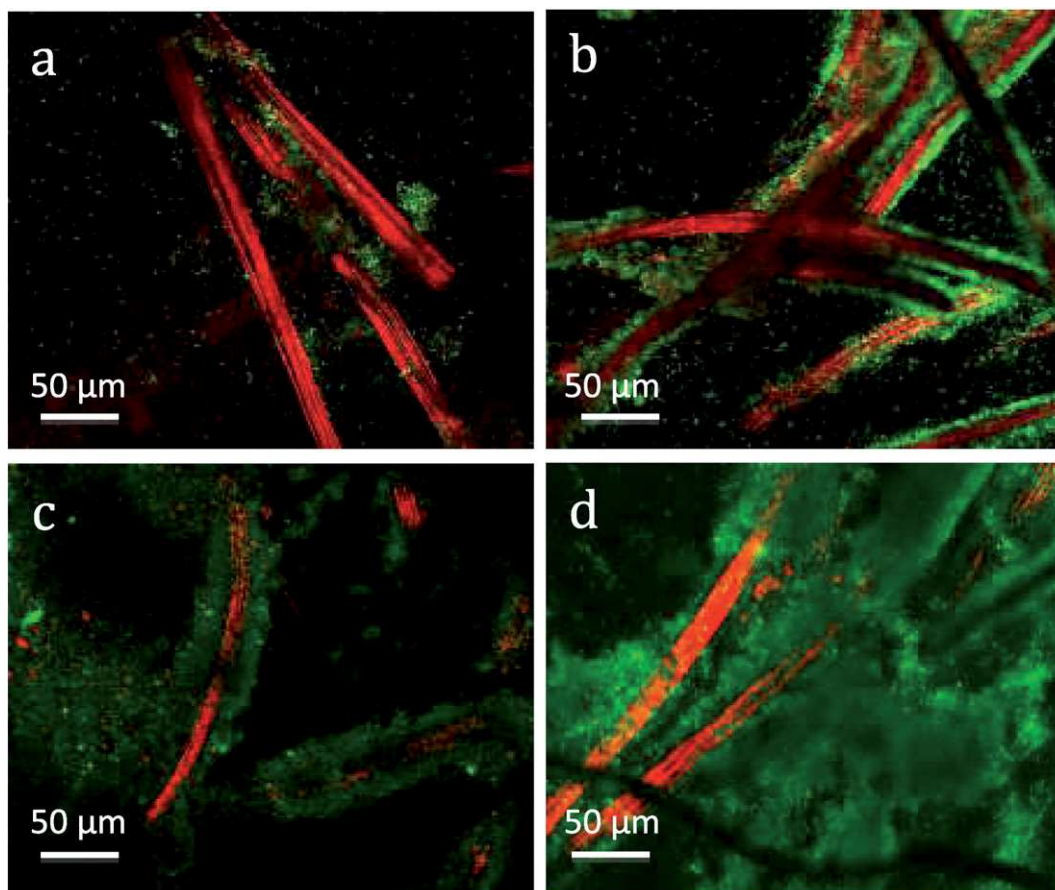
Fig. 4. CLSM images of biofilms stained with SYTO®9. Excitation 488 and 647 nm, emission 560–590 nm (green channel) and 585–640 nm (red channel). Z sections were acquired with 1 μm step. Bioanodes developed on graphite felt anodes polarized at different potentials/SCE (experimental run #5): a) V = −0.4 V, J = 8 A/m², Projection of Z-sections 8 μm; b) V = −0.2 V, J = 18 A/m², single slice; c) V = −0 V, J = 31 A/m², single slice; d) V = 0.2 V, J = 39 A/m². Projection of Z-sections 35 μm.

correlation between the electrochemical properties and the percentage of *Desulfuromonas* spp. (Fig. 6). The theoretical maximal current j_{Max} increased with the *Desulfuromonas* percentage and then stabilized when *Desulfuromonas* made up more than about 20–30% of the microbial community. Their role in electroactivity can consequently be assumed.

3.4. Comparison with data reported for other microbial anodes

Electroanalytical studies devoted to the impact of the polarization potential on the formation of multispecies bioanodes and performed in well-controlled electrochemical conditions are not very numerous, and the reported results do not reveal clear trends. Review articles have commented on this context recently [4,31].

From the point of view of the current density produced, some bioanodes have shown increasing performance when the applied potential value was increased [19,22], while others have revealed an optimal value, with lower performance above and below this value [32–34]. Potential-independent performance has been observed [24] and exactly opposite behaviour has also been experienced, i.e. higher current density at the lowest formation potential value [20]. Actually, the different potential ranges and inocula that have been used in the various studies may well be a source of large variation in the results reported.

Attempts to assess the impact of the applied potential on the selection of microbial families, genera or species have not shown clearer trends. Bioanodes formed from activated sludge have revealed the predominance of *Geobacter* sp. at −0.39 V/SCE, while a large microbial diversity was observed at higher formation potential values [20].

Similarly, the lowest applied potential has led to the selection of a single dominant species (*Desulfuromonas acetexigens*) in bioanodes formed from raw paper mill effluents [30].

In contrast, other studies have reported that the microbial communities do not depend on the potential applied to develop them. Microbial anodes formed at −0.4, −0.2 and 0.1 V/SCE from garden compost provided identical performance and DGGE has evidenced the same three dominant groups: *Geobacter*, *Anaerophaga* and *Pelobacter*, whatever the applied potential [24]. Nevertheless, the redox systems contained in the biofilms showed some differences depending on the potential. Microbial anodes formed from wastewater have also shown similar biofilm communities dominated by bacteria most similar to *Geobacter sulfurreducens*, whatever was the applied potential [25]. (See also the discussion about this work: [35], and [36]).

A study that used a mixture of soil and activated sludge as inoculum designed *Geobacter*-dominated bioanodes, showing that selection by potential acted at the species level. A strain of *G. psychrophilus* was dominant at −0.25 V vs. Ag/AgCl but was genetically different from the strains that dominated the −0.42 and −0.36 V bioanodes [23]. This article also reported that just changing a few operating parameters (batch vs. continuous, temperature, buffer concentration, nitrogen feeding or not) could lead to different bioanodes, no longer *Geobacter*-dominated. This article pointed out the difficulty of drawing general conclusions on this issue.

The only rule that seems to be widely evoked is that high potential values may support the growth of numerous, even moderately efficient, electroactive species while lower potential may favour the selection of
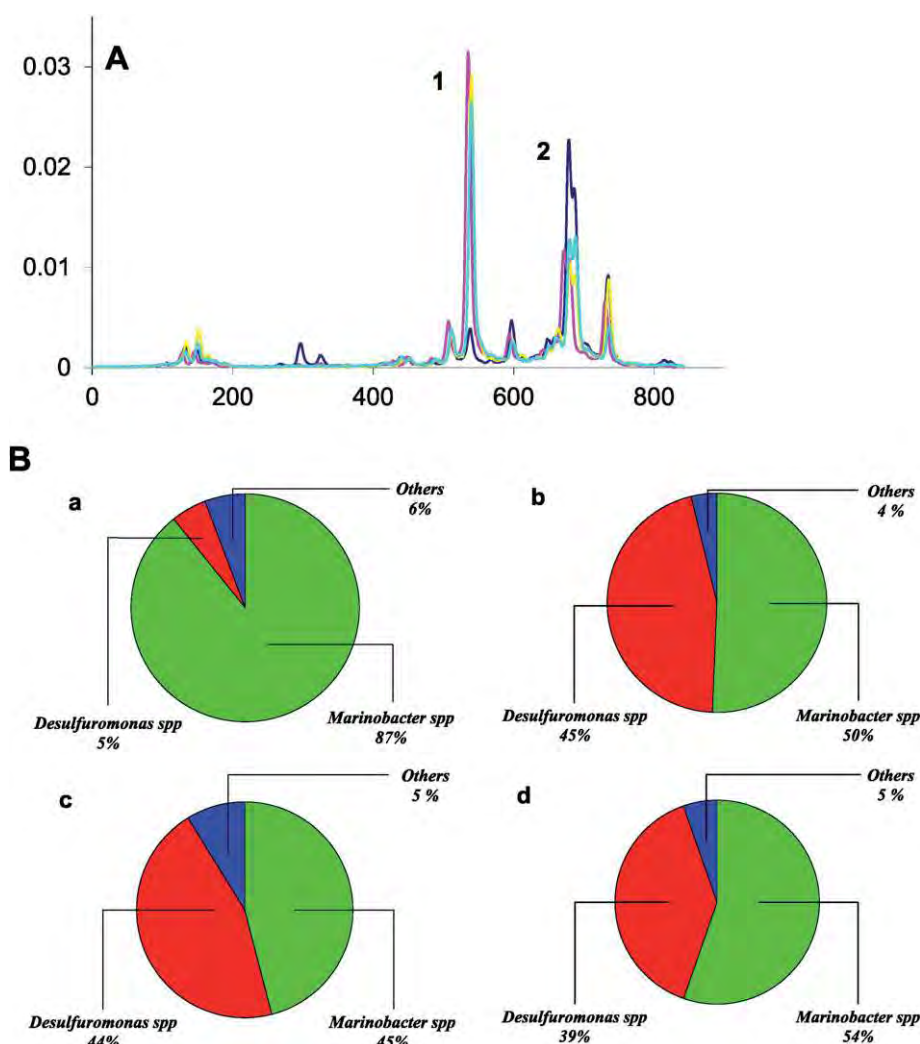
Fig. 5. Analysis of the microbial communities of four bioanodes formed at different applied potentials (run #5). A. Superimposed CE-SSCP profiles of the four bioanodes, dark blue −0.4 V, pink −0.2 V, yellow 0.0 V, and cyan 0.2 V/SCE. The fluorescence intensity (in arbitrary unit) is given as a function of the retention time (in number of scans); the numerical values depend on the equipment and can be used only to compare different samples in exactly the same operating conditions. B. 16S rRNA gene pyrosequencing of the bioanodes formed at a. −0.4 V; b. −0.2 V; c. 0.0 V; d. 0.2 V/SCE.

the most efficient electroactive species that are able to exploit the small difference between the anode potential (electron acceptor) and the redox potential of the substrate (electron donor).
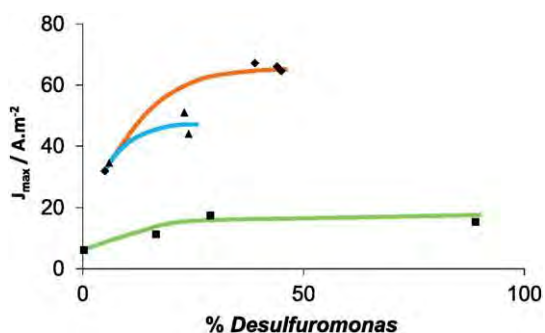

Fig. 6. Maximal current density extracted from the Butler-Volmer-Monod model as a function of the percentage of *Desulfuromonas* spp. determined by 16S rRNA gene pyrosequencing. Squares: run #4 from this work, diamonds: run #5 from this work, triangles: data extracted from Rousseau et al. [11]), these data did not use J_{Max}, which was not available, but the current provided by the bioanodes just before they were collected.

Here, the experimental conditions are markedly different from the previous studies because of the very high salinity of the medium. Halotolerant bioanodes formed from salt marsh have shown stringent and reproducible selection of only two genera, *Marinobacter* and *Desulfuromonas* [11], which is original behaviour, not reported so far with other kinds of multispecies bioanodes. The present study showed that the applied potential impacted the microbial community mainly at the lowest value (−0.4 V/SCE), selecting *Marinobacter* spp. as very dominant species but with a weaker colonization of the electrode surface. According to the literature analysis above, it may be guessed that the *Marinobacter* genus contains the most efficient electroactive species, which are able to implement anode respiration at low applied potential. This deduction is confirmed by the analysis of the experimental data presented below.

3.5. Electrochemical kinetics, biofilm structure and microbial composition support a speculative scenario of bioanode formation

During the voltammetry, the bioanodes formed at −0.4 V/SCE produced the highest currents in the range of low potential (below about 0.0 V/SCE). They could consequently be considered as more efficient than the other bioanodes in the low potential range. Biofilm imaging showed a considerably weaker colonization in comparison to the

bioanodes formed under the highest potentials. The bioanodes formed at −0.4 V/SCE displayed higher currents while remaining considerably less colonized. It must be concluded that very efficient electroactive species were present in the rare colonized patches. The low value of K_1 extracted from the Butler-Volmer-Monod kinetics for these bioanodes confirmed a faster electron transfer process. Analysis of the microbial community showed that *Marinobacter* spp., largely dominant (87 and 93.5%), were responsible for the higher electron transfer performance.

The J_{Max} parameter values extracted from Butler-Volmer-Monod kinetics showed a unitary trend, with a lower value for the bioanodes formed at −0.4 V/SCE. The bioanodes formed at −0.4 V/SCE showed better electron transfer but they led to lower average J_{Max}. Analysis of the microbial communities indicated that the value of J_{max} was correlated with the proportion of *Desulfuromonas* spp. An increased J_{Max} corresponded to a higher percentage of *Desulfuromonas* spp., up to a saturation threshold in the range of 20–30%, above which the *Desulfuromonas* spp. increase no longer impacted the J_{Max} value. Biofilm imaging showed an enhanced colonization of the surface of the bioanodes formed under high potentials.

In summary, *Marinobacter* spp. displayed higher electron transfer capability, but obtaining higher J_{max} values required the growth of *Desulfuromonas* spp. The electrodes formed at −0.4 V/SCE showed poor surface colonization. The potential of −0.4 V/SCE was not high enough to support significant development of *Desulfuromonas* spp., but *Marinobacter* spp., which was largely dominant at this potential, was not able to ensure widespread surface colonization. It can consequently be assumed that *Marinobacter* spp. achieved more effective electron transfer than *Desulfuromonas* spp., but it hardly grew without significant development of *Desulfuromonas* spp.

This scenario was supported by the crossed analyses of the electrochemical kinetics, the biofilm structures and the microbial communities and gives a consistent explanation to a set of complex experimental data. The fact that the experiments were reproduced five times, using different samples of the inoculum, with large inoculum amounts, increased the variability of the raw experimental data but allowed the conclusions to be considered as characteristic of the inoculum. The strong selection of only two dominant microbial genera at a ratio that depended on the applied potential was thus shown to be reproducible, even using different inoculum samples.

Further experiments with co-cultures of defined species of *Desulfuromonas* and *Marinobacter* are now necessary to confirm or correct the proposed scenario. Moreover, this scenario suggests a track to further enhancement of the efficiency of halotolerant bioanodes by favouring the electrode surface colonization by *Marinobacter* spp., which achieved more efficient electron transfer than *Desulfuromonas* spp., either by growing a pure culture of *Marinobacter* spp., or keeping the *Desulfuromonas* spp. ratio at the minimum required to form a dense biofilm.

4. Conclusions

The 20 bioanodes analysed in this study associated with experiments reported previously emphasize the stringent and reproducible selection of the two genera *Desulfuromonas* and *Marinobacter* in halotolerant electroactive biofilms. *Desulfuromonas* spp. have already been identified in electroactive biofilms but, to our knowledge, the *Marinobacter* genus has not been identified as a source of electroactive species yet.

A tentative scenario of bioanode formation is proposed, showing different contributions from each of the two genera. According to this scenario, *Marinobacter* spp. should provide remarkably efficient electroactive species, but they are not able to colonize the electrode surface broadly at low potential, in the absence of *Desulfuromonas* spp. *Marinobacter* spp. should now be considered as an essential candidate to design efficient microbial anodes able to operate in high-salinity electrolytes, with the help of *Desulfuromonas* spp. to enhance biofilm development on the electrode surface.

Appendix A. Supplementary data

Supplementary data to this article can be found online at http://dx.doi.org/10.1016/j.bioelechem.2016.06.006.

References

[1] D. Pant, A. Singh, G. Van Bogaert, S.I. Olsen, P.S. Nigam, L. Diels, K. Vanbroekhoven, Bioelectrochemical systems (BES) for sustainable energy production and product recovery from organic wastes and industrial wastewaters, RSC Adv. 2 (2012) 1248–1263.

[2] H. Wang, Z.J. Ren, A comprehensive review of microbial electrochemical systems as a platform technology, Biotechnol. Adv. 31 (2013) 1796–1807.

[3] A.P. Borole, G. Reguera, B. Ringeisen, Z.-W. Wang, Y. Feng, B.H. Kim, Electroactive biofilms: current status and future research needs, Energy Environ. Sci. 4 (2011) 4813–4834.

[4] M. Rimboud, D. Pocaznoi, B. Erable, A. Bergel, Electroanalysis of microbial anodes for bioelectrochemical systems: basics, progress and perspectives, Phys. Chem. Chem. Phys. 16 (2014) 16349–16366.

[5] X. Xie, C. Criddle, Y. Cui, Design and fabrication of bioelectrodes for microbial bioelectrochemical systems, Energy Environ. Sci. 8 (2015) 3418–3441.

[6] S.F. Ketep, A. Bergel, A. Calmet, B. Erable, Stainless steel foam increases the current produced by microbial bioanodes in bioelectrochemical systems, Energy Environ. Sci. 7 (2014) 1633–1637.

[7] D. Pocaznoi, A. Calmet, L. Etcheverry, B. Erable, A. Bergel, A. Stainless steel is a promising electrode material for anodes of microbial fuel cells, Energy Environ. Sci. 5 (2012) 9645–9652.

[8] A. Baudler, I. Schmidt, M. Langner, A. Greiner, U. Schroder, Does it have to be carbon? Metal anodes in microbial fuel cells and related bioelectrochemical systems, Energy Environ. Sci. 8 (2015) 2048–2055.

[9] S. Chen, G. He, Q. Liu, F. Harnisch, Y. Zhou, Y. Chen, M. Hanif, S. Wang, X. Peng, H. Hou, U. Schröder, Layered corrugated electrode macrostructures boost microbial bioelectrocatalysis, Energy Environ. Sci. 5 (2012) 9769–9772.

[10] R. Rousseau, X. Dominguez-Benetton, M.-L. Delia, A. Bergel, Microbial bioanodes with high salinity tolerance for microbial fuel cells and microbial electrolysis cells, Electrochem. Commun. 33 (2013) 1–4.

[11] R. Rousseau, C. Santaella, A. Wafa, J.-J. Godon, A. Bonnafous, A. Bergel, M.-L. Delia, Correlation of the electrochemical kinetics of high-salinity-tolerant bioanodes with the structure and microbial composition of the biofilm, ChemElectroChem 1 (2014) 1966–1975.

[12] M. Mehanna, R. Basseguy, M.-L. Delia, A. Bergel, Role of direct microbial electron transfer in corrosion of steels, Electrochem. Commun. 11 (2009) 568–571.

[13] M.L. Carvalho, J. Doma, M. Sztyler, I. Beech, P. Cristiani, The study of marine corrosion of copper alloys in chlorinated condenser cooling circuits: the role of microbiological components, Bioelectrochemistry 97 (2014) 2–6.

[14] L.E. Chavez de Paz, G. Bergenholtz, G. Svensater, The effects of antimicrobials on endodontic biofilm bacteria, J. Endod. 36 (2010) 70–77.

[15] J.J. Godon, E. Zumstein, P. Dabert, F. Habouzit, R. Moletta, Molecular microbial diversity of an anaerobic digestor as determined by small-subunit rDNA sequence analysis, Appl. Environ. Microbiol. 63 (1997) 2802–2813.

[16] C. Delbes, R. Moletta, J.J. Godon, Monitoring of activity dynamics of an anaerobic digester bacterial community using 16S rRNA polymerase chain reaction — single-strand conformation polymorphism analysis, Environ. Microbiol. 2 (2000) 506–515.

[17] N. Wery, V. Bru-Adan, C. Minervini, J.P. Delgenes, L. Garrelly, J.J. Godon, Dynamics of *Legionella* spp. and bacterial populations during the proliferation of *L. pneumophila* in a cooling tower facility, Appl. Environ. Microbiol. 74 (2008) 3030–3037.

[18] R.J. Michelland, S. Dejean, S. Combes, L. Lamothe, L. Cauquil, StatFingerprints: a friendly graphical interface program for processing and analysis of microbial fingerprint profiles, Mol. Ecol. Resour. 9 (2009) 1359–1363.

[19] D.A. Finkelstein, L.M. Tender, J.G. Zeikus, Effect of electrode potential on electrode-reducing microbiota, Environ. Sci. Technol. 40 (2006) 6990–6995.

[20] C.I. Torres, R. Krajmalnik-Brown, P. Parameswaran, A.K. Marcus, G. Wanger, Y.A. Gorby, B.E. Rittmann, Selecting anode-respiring bacteria based on anode potential: phylogenetic, electrochemical, and microscopic characterization, Environ. Sci. Technol. 43 (2009) 9519–9524.

[21] E. Marsili, J. Sun, D.R. Bond, Voltammetry and growth physiology of *Geobacter sulfurreducens* biofilms as a function of growth stage and imposed electrode potential, Electroanalysis 22 (2010) 865–874.

[22] X. Zhu, J.C. Tokash, Y. Hong, B.E. Logan, Controlling the occurrence of power overshoot by adapting microbial fuel cells to high anode potentials, Bioelectrochemistry 90 (2013) 30–35.

[23] A.S. Commault, G. Lear, M.A. Packer, R.J. Weld, Influence of anode potentials on selection of Geobacter strains in microbial electrolysis cells, Bioresour. Technol. 139 (2013) 226–234.

[24] B. Cercado, N. Byrne, M. Bertrand, D. Pocaznoi, M. Rimboud, W. Achouak, A. Bergel, Garden compost inoculum leads to microbial bioanodes with potential-independent characteristics, Bioresour. Technol. 134 (2013) 276–284.

[25] X. Zhu, M.D. Yates, M.C. Hatzell, H.A. Rao, P.E. Saikaly, B.E. Logan, Microbial community composition is unaffected by anode potential, Environ. Sci. Technol. 48 (2014) 1352–1358.

[26] H.V.M. Hamelers, A. ter Heijne, N. Stein, R.A. Rozendal, C.J.N. Buisman, Butler-Volmer-Monod model for describing bio-anode polarization curves, Bioresour. Technol. 102 (2011) 381–387.

[27] S.F. Wang, T. Chen, Z.L. Zhang, X.C. Shen, Z.X. Lu, D.W. Pang, K.Y. Wong, Direct electrochemistry and electrocatalysis of heme proteins entrapped in agaros hydrogel films in room-temperature ionic liquids, Langmuir 21 (2005) 9260–9266.

[28] R. Bond, D.E. Holmes, L.M. Tender, D.R. Lovley, Electrode-reducing microorganisms that harvest energy from marine sediments, Science 295 (2002) 483–485.

[29] T. Zhang, T.S. Bain, M.A. Barlett, S.A. Dar, O.L. Snoeyenbos-West, K.P. Nevin, D.R. Lovley, Sulfur oxidation to sulfate coupled with electron transfer to electrodes by *Desulfuromonas* strain TZ1, Microbiology 160 (2014) 1123–1129.

[30] S.F. Ketep, A. Bergel, M. Bertrand, A. Achouak, E. Fourest, Lowering the applied potential during successive scratching/re-inoculation improves the performance of microbial anodes for microbial fuel cells, Bioresour. Technol. 127 (2013) 448–455.

[31] R.C. Wagner, D.F. Call, B.E. Logan, Optimal set anode potentials vary in bioelectrochemical systems, Environ. Sci. Technol. 44 (2010) 6036–6041.

[32] P. Aelterman, S. Freguia, J. Keller, W. Verstraete, K. Rabaey, The anode potential regulates bacterial activity in microbial fuel cells, Appl. Microbiol. Biotechnol. 78 (2008) 409–418.

[33] S. Parot, M.-L. Delia, A. Bergel, Forming electrochemically active biofilms from garden compost under chronoamperometry, Bioresour. Technol. 99 (2008) 4809–4816.

[34] X. Wang, Y. Feng, J. Liu, H. Lee, N. Ren, Performance of a batch two-chambered microbial fuel cell operated at different anode potentials, J. Chem. Technol. Biotechnol. 86 (2010) 590–594.

[35] A.S. Commault, G. Lear, R.J. Weld, Comment on microbial community composition is unaffected by anode potential, Environ. Sci. Technol. 48 (2014) 14851–14852.

[36] X. Zhu, M.D. Yates, M.C. Hatzell, H.A. Rao, P.E. Saikaly, B.E. Logan, Response to comment on microbial community composition is unaffected by anode potential, Environ. Sci. Technol. 48 (2014) 14853–14854.